spectrum (Figure 2) in the 19-23-eV IE region.

ΔSCF ab initio IE values (Table IV) provide an accurate fitting of experimental IE values. Thus, bands a and b represent the ionization of 9a″ (π_4) and 8a″ (π_3) MOs, while bands c-e represent the ionization of 22a′, 21a′, and 7a″ MOs, respectively.

This assignment is consistent with previous PE data for closely related species, including several Tl(I) complexes.[21] It is noted, however that the IE presently attributed to 22a′ MO represents the lowest value reported to date[21,22] for $6s^{-1}$ ionization in Tl(I) compounds (Table IV). Besides the effects due to the partial charge on the Tl atom and with the assumption of no differential relaxation energies upon ionization among the various Tl(I) complexes, this observation points to a more extensive covalent 6s-a′ mixing.

Finally, we discuss the higher IE doublet (x, x′ in Figure 2) structure. Reference to literature data clearly indicates that the features must be related to the $^2D_{5/2}$ and $^2D_{3/2}$ multiplet states produced upon production of the ionized $5d^9$ configuration of the metal center.[21,22a] As already observed for other "covalent" Tl(I) complexes,[21] there is no evidence of any fine structure due to "ligand field" splitting, which, conversely, proved ubiquitous in the spectra of Tl(I) halides.[22a] This observation points to a "corelike" behavior of 5d subshells mostly sensitive to electrostatic perturbations rather than to covalent mixing involving differential overlaps. Finally, the average metal 5d IE (20.45 eV) is close to the lowest value observed to date for $Tl(HB(pz)_3)$[21b] and consistently lower than the value observed for the Tl atom.[22a] This "chemical shift" has, however, been interpreted in terms of "extraatomic" relaxation due to the more polarizable ligand framework.[21c]

Acknowledgment. We thank the Consiglio Nazionale delle Ricerche (CNR, Rome) and the Ministero dell'Università e della Ricerca Scientifica e Tecnologica (MURST, Rome) for financial support.

Registry No. I, 139377-73-4; pyrrole-2-carboxaldehyde, 1003-29-8; *tert*-butylamine, 75-64-9.

(21) (a) Bruno, G.; Centineo, G.; Ciliberto, E.; Fragalà, I. *J. Electron Spectrosc. Relat. Phenom.* **1983**, *32*, 153. (b) Bruno, G.; Ciliberto, E.; Fragalà, I.; Granozzi, G. *Inorg. Chim. Acta* **1981**, *48*, 61. (c) Egdell, R. G.; Fragalà, I.; Orchard, A. F. *J. Electron Spectrosc. Relat. Phenom.* **1978**, *14*, 467.

(22) (a) Egdell, R. G.; Orchard, A. F. *J. Chem. Soc., Faraday Trans. 2* **1978**, *74*, 1179. (b) Ruscic, B.; Goodman, G. L.; Berkowitz, J. *J. Electron Spectrosc. Relat. Phenom.* **1986**, *41*, 357.

Contribution from the Department of Chemistry, Faculty of Engineering, Gifu University, Yanagido, Gifu 501-11, Japan, Institute for Molecular Science, Myodaiji, Okazaki 444, Japan, and Department of Chemistry, Faculty of Science, Tohoku University, Aramaki, Aoba-ku Sendai 980, Japan

Synthesis, Structure, and Properties of Oxidized Hexamolybdenum Clusters $[(Mo_6X_7Y)X'_6]^{2-}$ (X = X′ = Cl, Br; Y = S, Se)

Masahiro Ebihara,*[1a] Kiyoshi Isobe,[1b] Yoichi Sasaki,[1c] and Kazuo Saito*[1b,d]

Received August 14, 1990

The synthesis, structure, and properties of $Mo_6(13+)$ species, which are obtained by the oxidation of $Mo_6(12+)$ species $[(Mo_6X_7Y)X'_6]^{3-}$ (X = X′ = Cl, Br; Y = S, Se), are reported. $(n\text{-}Bu_4N)_2[(Mo_6Cl_7S)Cl_6]$ crystallizes in the monoclinic space group $P2_1/n$ with a = 18.542 (2) Å, b = 11.701 (2) Å, c = 12.806 (2) Å, β = 90.21 (1)°, V = 2778.5 (7) Å^3, and Z = 2. $(n\text{-}Bu_4N)_2[(Mo_6Cl_7Se)Cl_6]$ crystallizes in the monoclinic space group $P2_1/n$ with a = 18.571 (2) Å, b = 11.685 (1) Å, c = 12.845 (1) Å, β = 90.12 (1)°, V = 2787.1 (5) Å^3, and Z = 2. $(n\text{-}Bu_4N)_2[(Mo_6Br_7S)Cl_6]$ also crystallizes in the monoclinic space group $P2_1/n$ with a = 18.740 (2) Å, b = 11.647 (2) Å, c = 13.030 (2) Å, β = 90.05 (1)°, V = 2844.0 (7) Å^3, and Z = 2. The $Mo_6(12+)$ species $(Et_4N)_3[(Mo_6Br_7S)Cl_6]$ crystallizes in the tetragonal space group $P4_2/mnm$ with a = 11.968 (1) Å, c = 16.804 (2) Å, V = 2406.8 (4) Å^3, and Z = 2. The Mo-Mo distances of the $Mo_6(13+)$ clusters (2.626 (3) Å in $[(Mo_6Cl_7S)Cl_6]^{2-}$, 2.628 (3) Å in $[(Mo_6Cl_7Se)Cl_6]^{2-}$, 2.653 (3) Å in $[(Mo_6Br_7S)Cl_6]^{2-}$) are slightly longer than those of the corresponding $Mo_6(12+)$ species. Absorption peak positions in the 1800-nm (5320-6060 cm^{-1}) and 900-nm regions (10 500-11 200 cm^{-1}) are independent of the capping and terminal ligands, but those in the range 480-650 nm (15 400-20 400 cm^{-1}) depend on the ligand. Their ESR spectra at 77 K are axially symmetric ($g_\perp$ = 2.12-2.15, $g_\parallel$ = 2.05-2.07). The electronic structure is discussed on the basis of these data.

Hexamolybdenum clusters provide various complexes with halides or chalcogenides as capping or terminal ligands. The complexes with eight capping halides $[(Mo_6X_8)X'_6]^{2-}$ (X = X′ = Cl, Br, I; Mo_6,12+), are discrete ions, give strong red emissions,[2,3] and are oxidized and reduced with difficulty.[2] On the other hand, those with eight capping chalcogenides, $Mo_6Y_8^{n-}$ (Y = S, Se, Te), are nonstoichiometric in the superconducting solid Chevrel phase, in which the total oxidation number of six molybdenum atoms is in the range 12+ to 16+.[4] (For convenience the oxidation number of Mo_6 moiety is expressed in parentheses after the moiety.) Although a variety of discrete hexamolybdenum clusters of $Mo_6(12+)$ were reported,[5-7] halide clusters with oxidized

(1) (a) Gifu University. (b) Institute for Molecular Science. (c) Tohoku University. (d) Present address: Graduate School, International Christian University, Osawa, Mitaka 181, Japan.

(2) (a) Maverick, A. W.; Najdzionek, J. S.; Mackenzie, D.; Nocera, D. G.; Gray, H. B. *J. Am. Chem. Soc.* **1983**, *105*, 1878. (b) Nocera, D. G.; Gray, H. B. *J. Am. Chem. Soc.* **1984**, *106*, 825.

(3) (a) Maverick, A. W.; Gray, H. B. *J. Am. Chem. Soc.* **1981**, *103*, 1298. (b) Tanaka, H. K.; Sasaki, Y.; Saito, K. *Sci. Pap. Inst. Phys. Chem. Res.* **1984**, *78*, 92. (c) Saito, Y.; Tanaka, H. K.; Sasaki, Y.; Azumi, T. *J. Phys. Chem.* **1985**, *89*, 4413. (d) Tanaka, H. K.; Sasaki, Y.; Ebihara, M.; Saito, K. *Inorg. Chim. Acta* **1988**, *161*, 63. (e) Kraut, K.; Ferraudi, G. *Inorg. Chem.* **1989**, *28*, 4578.

(4) (a) Chevrel, R.; Sergent, M.; Prigent, J. *J. Solid State Chem.* **1971**, *3*, 515. (b) Yvon, K. *Current topics in Material Science*, 1st ed.; Kaldis, E., Ed.; North Holland Publishing Co.: New York, 1978; Vol. 3, Chapter 2.

(5) (a) Sheldon, J. C. *Nature* **1959**, *184*, 1210. (b) Sheldon, J. C. *J. Chem. Soc.* **1960**, 1007. (c) Sheldon, J. C. *J. Chem. Soc.* **1962**, 410. (d) Cotton, F. A.; Curtis, N. F. *Inorg. Chem.* **1965**, *4*, 241. (e) Cotton, F. A.; Wing, R. M.; Zimmerman, R. A. *Inorg. Chem.* **1967**, *6*, 11. (f) Fergusson, J. E.; Robinson, B. H.; Wilkins, C. J. *J. Chem. Soc. A* **1967**, 486. (g) Nannelli, P.; Block, P. *Inorg. Chem.* **1968**, *7*, 2423. (h) Hamer, A. D.; Smith, T. J.; Walton, R. A. *Inorg. Chem.* **1976**, *15*, 1014. (i) Weissenhorn, R. G. *Z. Anorg. Allg. Chem.* **1976**, *426*, 159. (j) von Schnering, H. G. *Z. Anorg. Allg. Chem.* **1971**, *385*, 75. (k) Schaffer, H.; Brendel, C.; Henkel, G.; Krebs, B. *Z. Anorg. Allg. Chem.* **1982**, *491*, 275. (l) Chisholm, M. H.; Heppert, J. A.; Huffuman, J. C. *Polyhedron* **1984**, *3*, 475. (m) Saito, T.; Nishida, M.; Yamagata, T.; Yamagata, Y.; Yamaguchi, Y. *Inorg. Chem.* **1986**, *25*, 1111. (n) Potel, M.; Perrin, C.; Perrin, A.; Sergent, M. *Mater. Res. Bull.* **1986**, *21*, 1239.

0020-1669/92/1331-1644$03.00/0

Table I. Crystal Data and Details of the Structure Determinations[a]

	Mo6(13+)			Mo6(12+)
	$(n\text{-}Bu_4N)_2[(Mo_6Cl_7S)Cl_6]$	$(n\text{-}Bu_4N)_2[(Mo_6Cl_7Se)Cl_6]$	$(n\text{-}Bu_4N)_2[(Mo_6Br_7S)Cl_6]$	$(Et_4N)_3[(Mo_6Br_7S)Cl_6]$
fw	1553.53	1600.42	1864.66	1770.48
a, Å	18.542 (2)	18.571 (2)	18.740 (2)	11.968 (1)
b, Å	11.701 (2)	11.685 (1)	11.647 (2)	
c, Å	12.806 (2)	12.845 (1)	13.030 (2)	16.804 (2)
β, deg	90.21 (1)	90.12 (1)	90.05 (1)	
V, Å^3	2778.5 (7)	2787.1 (5)	2844.0 (7)	2406.8 (4)
space group	$P2_1/n$	$P2_1/n$	$P2_1/n$	$P4_2/mnm$
Z	2	2	2	2
ρ_{calcd}, g cm^{-3}	1.86	1.91	2.18	2.44
μ, cm^{-1}	19.77	25.82	64.73	76.41
T, °C	25	25	25	25
λ(Mo Kα), Å	0.71073	0.71073	0.71073	0.71073
R	0.044	0.044	0.052	0.049
R_w	0.055	0.057	0.059	0.054

[a] Agreement factors defined as $R = \sum||F_o| - |F_c||/\sum|F_o|$ and $R_w = [\sum w(|F_o| - |F_c|)^2/\sum w|F_o|^2]^{1/2}$ with $w = [\sigma^2 + (0.02|F_o|)^2]^{-1}$.

molybdenum cores have not been isolated. Oxidized discrete clusters with eight capping chalcogenide ligands, $[(Mo_6Y_8)(PEt_3)_6]$ (Mo_6,16+) and $[(Mo_6Y_8)(PEt_3)_6]^-$ (Mo_6,15+) (Y = S, Se; Et = C_2H_5), were synthesized by Saito et al.,[8] but discrete Mo_6(13+) and Mo_6(14+) species are not known. We reported the synthesis, structure, and properties of hexamolybdenum cluster complexes with mixed capping ligands, one chalcogenide and seven halides.[9] These cluster complexes were found to be oxidized more easily than those with eight capping halides. We now report the synthesis, structure, and properties of such discrete Mo_6(13+) species.

Experimental Section

Reagents. Acetonitrile and dichloromethane for electrochemical measurements were distilled twice with P_2O_5 and once with CaH_2, respectively. Other reagents were of guaranteed grade and used without further purification. Complexes with Mo_6(12+) cores, $(n\text{-}Bu_4N)_3[(Mo_6X_7Y)Cl_6]$ (X, Y = Cl, S; Cl, Se; Br, S; Mo_6,12+) (Bu = C_4H_9), were prepared by the literature method.[9]

Syntheses. **$(n\text{-}Bu_4N)_2[(Mo_6Cl_7S)Cl_6]$ (Mo_6,13+).** $(n\text{-}Bu_4N)_3[(Mo_6Cl_7S)Cl_6]$ (Mo_6,12+) (100 mg) was dissolved in 30 cm^3 of concentrated HCl/CH_3OH (1/10 v/v). Aqueous bromine was dripped with stirring until a red precipitate formed. This was filtered off, washed with 20% aqueous HCl, and dried in vacuo. Yield: 75%. Anal. Calcd for $C_{32}H_{72}N_2Cl_{13}Mo_6S$: C, 24.74; H, 4.67; N, 1.80; Cl 29.67. Found: C, 24.68; H, 4.59; N, 1.80; Cl, 29.41.

$(n\text{-}Bu_4N)_2[(Mo_6Cl_7S)Br_6]$ (Mo_6,13+). Aqueous bromine was added to the HBr/CH_3OH (1/10 v/v) solution of $(n\text{-}Bu_4N)_3[(Mo_6Cl_7S)Cl_6]$ (Mo_6,12+) (100 mg). The black crystals were filtered off after 12 h, washed with 20% aqueous HBr, and dried in vacuo. Yield: 80%. Anal. Calcd for $C_{32}H_{72}N_2Br_6Cl_7Mo_6S$: C, 21.22; H, 3.99; N, 1.54. Found: C, 21.51; H, 4.01; N, 2.06.

$(n\text{-}Bu_4N)_2[(Mo_6Cl_7Se)Cl_6]$ (Mo_6,13+). $(n\text{-}Bu_4N)_3[(Mo_6Cl_7Se)Cl_6]$ (Mo_6,12+) was dissolved in concentrated HCl/CH_3OH (1/10 v/v). Concentrated HNO_3 was added dropwise to the solution until the solution turned green. The green precipitate was filtered off, washed with 20% aqueous HCl, and dried in vacuo. Yield: 70%. Anal. Calcd for $C_{32}H_{72}N_2Cl_{13}Mo_6Se$: C, 24.02; H, 4.53; N, 1.75. Found: C, 23.82; H, 4.50; N, 1.76.

$(n\text{-}Bu_4N)_2[(Mo_6Cl_7Se)Br_6]$ (Mo_6,13+). This complex was prepared by a method similar to that for $(n\text{-}Bu_4N)_2[(Mo_6Cl_7Se)Cl_6]$ by use of HBr instead of HCl. Yield: 72%. Anal. Calcd for $C_{32}H_{72}N_2Br_6Cl_7Mo_6Se$: C, 20.59; H, 3.89; N, 1.50. Found: C, 20.61; H, 3.88; N, 1.54.

$(n\text{-}Bu_4N)_2[(Mo_6Br_7S)Cl_6]$ (Mo_6,13+). This was prepared from $(n\text{-}Bu_4N)_3[(Mo_6Br_7S)Cl_6]$ by a similar method to that for $(n\text{-}Bu_4N)_2[(Mo_6Cl_7S)Cl_6]$. Yield 88%. Anal. Calcd for $C_{32}H_{72}N_2Br_7Cl_6Mo_6S$: C, 20.61; H, 4.17; N, 1.50. Found: C, 20.53; H, 3.79; N, 2.07.

X-ray Structure Determination. $(n\text{-}Bu_4N)_2[(Mo_6X_7Y)Cl_6]$ (X, Y = Cl, S; Cl, Se; Br, S; Mo_6,13+). Single crystals of $(n\text{-}Bu_4N)_2[(Mo_6Cl_7S)Cl_6]$ (Mo_6,13+) and $(n\text{-}Bu_4N)_2[(Mo_6Cl_7Se)Cl_6]$ (Mo_6,13+) were obtained by layering hexane on dichloromethane solution of the complexes. $(n\text{-}Bu_4N)_2[(Mo_6Br_7S)Cl_6]$ (Mo_6,13+) was crystallized from hot concentrated HCl/CH_3OH (1/10 v/v) solution. Intensity data were collected on a Rigaku AFC-5 or AFC-5R four-circle diffractometer at 25 °C by use of the θ–2θ scan technique and graphite-monochromated Mo Kα

Table II. Final Positional Parameters and B_{eq} Values (Å^2) for the Significant Atoms of $(n\text{-}Bu_4N)_2[(Mo_6Cl_7S)Cl_6]$ (Mo_6,13+)[a]

atom	x	y	z	B_{eq}[b]
Mo(1)	8507 (3)	6373 (5)	4885 (4)	3.13 (1)
Mo(2)	4882 (3)	−13450 (5)	−3136 (4)	3.24 (1)
Mo(3)	1927 (3)	5421 (5)	−13339 (4)	3.31 (1)
X(1)	5241 (9)	23750 (15)	−5072 (14)	4.41 (4)
X(2)	10697 (8)	−11875 (15)	14155 (12)	3.96 (4)
X(3)	−1655 (9)	−13619 (16)	−20015 (12)	4.39 (5)
X(4)	14414 (8)	−1333 (16)	−10790 (12)	4.25 (4)
Cl(1)	19657 (9)	14521 (16)	11428 (15)	4.95 (5)
Cl(2)	11261 (10)	−30784 (17)	−7738 (17)	5.69 (6)
Cl(3)	4307 (11)	11892 (20)	−30981 (14)	6.03 (6)

[a] Positional parameters have been multiplied by 10^5. [b] $B_{eq} = {}^3/_4[\sum_i\sum_j\beta_{ij}a_ia_j]$.

Table III. Final Positional Parameters and B_{eq} Values (Å^2) for the Significant Atoms of $(n\text{-}Bu_4N)_2[(Mo_6Cl_7Se)Cl_6]$ (Mo_6,13+)[a]

atom	x	y	z	B_{eq}[b]
Mo(1)	8477 (3)	6406 (6)	4913 (5)	2.96 (2)
Mo(2)	4886 (3)	−13489 (6)	−3117 (5)	3.05 (2)
Mo(3)	1960 (3)	5447 (6)	−13302 (5)	3.12 (2)
X(1)	5249 (9)	24042 (15)	−5072 (14)	4.19 (5)
X(2)	10727 (8)	−12141 (14)	14336 (12)	3.40 (4)
X(3)	−1586 (9)	−13727 (16)	−20103 (13)	4.35 (5)
X(4)	14493 (9)	−1317 (18)	−10768 (14)	4.69 (5)
Cl(1)	19591 (11)	14562 (19)	11479 (18)	4.96 (6)
Cl(2)	11252 (13)	−30802 (21)	−7658 (20)	5.76 (7)
Cl(3)	4414 (13)	11873 (25)	−30857 (17)	6.11 (8)

[a] Positional parameters have been multiplied by 10^5. [b] $B_{eq} = {}^3/_4[\sum_i\sum_j\beta_{ij}a_ia_j]$.

Table IV. Final Positional Parameters and B_{eq} Values (Å^2) for the Significant Atoms of $(n\text{-}Bu_4N)_2[(Mo_6Br_7S)Cl_6]$ (Mo_6,13+)[a]

atom	x	y	z	B_{eq}[b]
Mo(1)	8381 (8)	6566 (15)	5211 (12)	3.05 (5)
Mo(2)	5034 (9)	−13448 (15)	−3088 (13)	3.10 (5)
Mo(3)	2153 (9)	5721 (16)	−13120 (12)	3.30 (5)
X(1)	5374 (12)	25352 (19)	−4796 (18)	4.32 (7)
X(2)	10965 (12)	−12631 (21)	14853 (17)	4.40 (7)
X(3)	−1240 (12)	−14127 (21)	−20908 (17)	4.42 (7)
X(4)	15164 (12)	−913 (23)	−10562 (18)	5.25 (7)
Cl(1)	19305 (27)	14658 (47)	12119 (43)	5.13 (18)
Cl(2)	11543 (29)	−30686 (49)	−7538 (45)	5.73 (19)
Cl(3)	4804 (31)	12494 (57)	−30312 (40)	6.29 (21)

[a] Positional parameters have been multiplied by 10^5. [b] $B_{eq} = {}^3/_4[\sum_i\sum_j\beta_{ij}a_ia_j]$.

(6) Okumura, H.; Taga, T.; Osaki, K.; Tsujikawa, I. *Bull. Chem. Soc. Jpn.* **1982**, *55*, 307.
(7) Ouahab, L.; Batail, P.; Perrin, C.; Garrigou-Laglange, C. *Mater. Res. Bull.* **1986**, *21*, 1223.
(8) (a) Saito, T.; Yamamoto, N.; Yamagata, T.; Imoto, H. *J. Am. Chem. Soc.* **1988**, *110*, 1646. (b) Saito, T.; Yamamoto, N.; Nagase, T.; Tsuboi, T.; Kobayashi, K.; Yamagata, T.; Imoto, H.; Unoura, K. *Inorg. Chem.* **1990**, *29*, 764.
(9) Ebihara, M.; Toriumi, K.; Saito, K. *Inorg. Chem.* **1988**, *27*, 13.

Table V. Final Positional Parameters and B_{eq} Values (Å^2) for the Significant Atoms of $(Et_4N)_3[(Mo_6Br_7S)Cl_6]$ (Mo_6,12+)[a]

atom	x	y	z	B_{eq}[b]
Mo(1)	7826 (4)	7826	7834 (4)	1.60 (1)
Mo(2)	10962 (6)	−10962	0	1.56 (2)
X(1)	10966 (6)	−10966	15528 (5)	2.43 (2)
X(2)	26209 (9)	4476 (9)	0	2.41 (3)
Cl(1)	18268 (16)	18268	18166 (15)	3.28 (4)
Cl(2)	25439 (19)	−25439	0	2.93 (6)

[a] Positional parameters have been multiplied by 10^5. [b] $B_{eq} = {}^3/_4[\sum_i\sum_j\beta_{ij}a_ia_j]$.

radiation (λ = 0.710 73 Å). The intensities were corrected for Lorentz polarization factors and absorption effects but not for extinction. The cell dimensions were determined by a least-squares calculation by using $25° < 2\theta < 30°$ values measured on the diffractometer. Crystallographic data are listed in Table I.

The three complex salts had isomorphous monoclinic unit cells (space group $P2_1/n$). The structure was solved with three-dimensional Patterson maps and refined by the full-matrix least-squares program RADIEL.[10] All non-hydrogen atoms were located from the successive Fourier syntheses and included in the refinement. The positions of capping chalcogenide atoms were not distinguished from those of capping halide atoms. Accordingly, all the capping atoms were refined with the scattering factor of ${}^1/_8Y + {}^7/_8X$. The scattering factors and anomalous scattering correction were taken from ref 11. Other crystal data correction and refinement parameters are summarized in Table I. The positional and equivalent thermal parameters of the clusters are listed in Tables II–IV.

$(Et_4N)_3[(Mo_6Br_7S)Cl_6]$ (Mo_6,12+). $(Et_4N)_3[(Mo_6Br_7S)Cl_6]$ (Mo_6,12+) (Et = C_2H_5) was crystallized by slow diffusion of an (n-$Bu_4N)_3[(Mo_6Br_7S)Cl_6]$ solution into a Et_4NCl solution. A vessel of 2-cm diameter was placed in a taller vessel of 3-cm diameter. The HCl/CH_3OH (1/10 v/v) solutions of (n-$Bu_4N)_3[(Mo_6Br_7S)Cl_6]$ and Et_4NCl were filled in the inner and the outer vessels, respectively. Large crystals grew on the wall of the inner vessel after 12 h. Intensity data were collected on a Rigaku AFC-5R four-circle diffractometer. Other conditions were similar to those for (n-$Bu_4N)_2[(Mo_6X_7Y)Cl_6]$. The systematic absence indicated that space group was $P4n2$, $P4_2nm$, or $P4_2/mnm$. The structure was solved of the centric space group $P4_2/mnm$ with Patterson maps. There are two sites of capping ligand (X(1) and X(2)) in an asymmetric unit. At first both of them were refined by the scattering factor of ${}^1/_8S + {}^7/_8Br$, but their thermal parameters were quite different. Then the population of sulfide and bromide at each site was also refined. Other crystal data correction and refinement parameters are summarized in Table I. The positional and equivalent thermal parameters of the cluster are listed in Table V.

Measurements. Absorption spectra were measured with a Hitachi 3400 spectrophotometer. ESR spectra were recorded on a JEOL FE2XG or JES2XG EPR spectrometer. Electrochemical measurements in CH_3CN and CH_2Cl_2 were carried out with a Yanaco P-1100 polarographic analyzer or a Hokuto HA-501G potentiostat/galvanostat and an HB-105 function generator. The working and the counter electrode were glassy carbon and platinum, respectively. Reference electrodes were Ag–$AgNO_3$ (0.1 M; M = mol dm^{-3}) in CH_3CN and Ag–AgCl in CH_2Cl_2. The supporting electrolyte was 0.1 M n-Bu_4NClO_4, and the sample concentration was 1×10^{-3} M. The potentials was related with the ferrocene/ferrocenium (Fc/Fc^+) couple.

Results and Discussion

Syntheses. We have pointed out that the capping ligands of Mo_6(12+) cluster complexes are replaced with much more difficulty than the terminal ligands. All the new complexes were prepared by the oxidation of Mo_6(12+) clusters with the given capping and terminal ligands. Bromine was used as an oxidizing reagent for the cluster complexes with capping sulfide, (n-$Bu_4N)_2[(Mo_6X_7S)X'_6]$ (X, X' = Cl, Cl; Cl, Br; Br, Cl; Br, Br), but not for those with capping selenide which were prepared by oxidation with nitric acid.

The oxidizing reagents were chosen on the basis of the oxidation potential. The aimed oxidized products were crystallized from the reaction mixture because of their low solubilities.

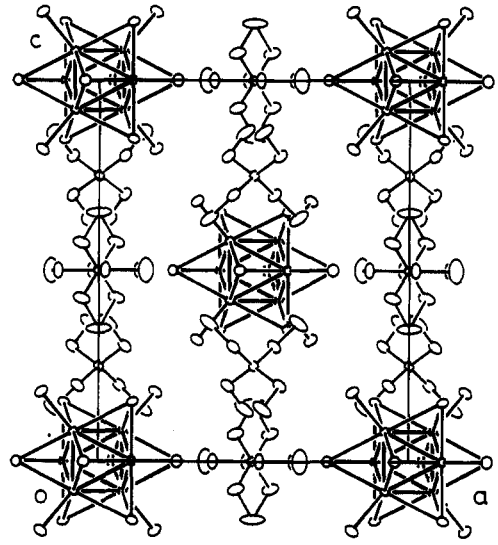

Figure 1. Crystal structure of $(Et_4N)_3[(Mo_6Br_7S)Cl_6]$ (Mo_6,12+). The thermal ellipsoids are drawn at 30% probability.

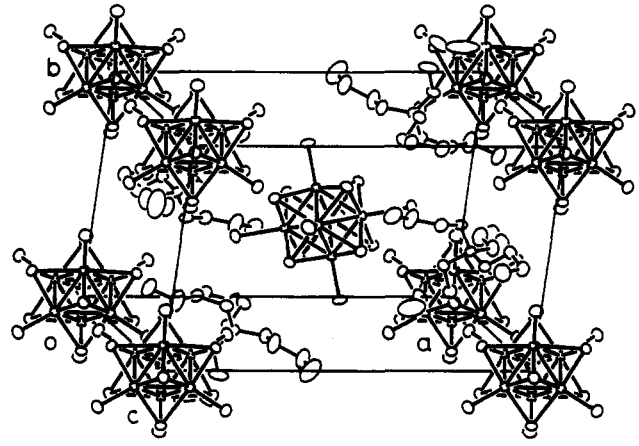

Figure 2. Crystal structure of (n-$Bu_4N)_2[(Mo_6Cl_7S)Cl_6]$ (Mo_6,13+). The thermal ellipsoids are drawn at 30% probability.

Table VI. Bond Distances (Å) and Angles (deg) of $(Et_4N)_3[(Mo_6Br_7S)Cl_6]$ (Mo_6,12+)[a]

Distances			
Mo(1)–Mo(2)	2.632 (1)	X(2)–Mo(1)	2.595 (1)
Mo(1)–Mo(1′)	2.649 (1)	X(2)–Mo(2)	2.597 (1)
Mo(1)–Mo(1″)	2.633 (1)	Mo(1)–Cl(1)	2.477 (2)
X(1)–Mo(1)	2.621 (1)	Mo(2)–Cl(2)	2.450 (2)
X(1)–Mo(2)	2.609 (1)		
Angles			
Mo(2)–Mo(1)–Mo(1′)	59.79 (2)	X(1)–Mo(1)–X(1′)	90.16 (2)
Mo(2)–Mo(1)–Mo(1″)	60.00 (1)	X(1)–Mo(1)–X(2)	89.78 (2)
Mo(1)–Mo(2)–Mo(1′)	60.42 (2)	X(1)–Mo(2)–X(2)	90.00 (3)
Mo(1)–Mo(2)–Mo(1″)	60.01 (1)	X(1)–Mo(1)–Cl(1)	90.85 (5)
Mo(1)–X(1)–Mo(1′)	60.71 (2)	X(2)–Mo(1)–Cl(1)	90.33 (5)
Mo(1)–X(1)–Mo(2)	60.43 (2)	X(1)–Mo(2)–Cl(2)	89.99 (4)
Mo(1)–X(2)–Mo(1″)	60.97 (3)	X(2)–Mo(2)–Cl(2)	90.36 (5)
Mo(1)–X(2)–Mo(2)	60.93 (3)		

[a] Key: (′) $-x, -y, z$; (″) $x, y, -z$.

Crystal and Molecular Structure. We reported the X-ray crystal structure of Mo_6 cluster complexes in the Mo_6(12+) state with mixed capping ligands.[9] The tetraethylammonium salt of one complex, $[(Mo_6Br_7S)Cl_6]^{3-}$, is now synthesized, and its crystal structure is given for comparison (Figure 1). Its bond distances and angles are listed in Table VI. The populations of sulfide and bromide at the two capping sites are not identical. The X(1) and X(2) sites consist of 5% S + 95% Br and 20% S + 80% Br, respectively. It is reasonable that the Mo–X(1) distances are longer than the Mo–X(2) distances.

(10) Coppens, P.; Guru Row, T. N.; Leung, P.; Stevens, E. D.; Becker, P. J.; Yang, Y. W. *Acta Crystallogr.* **1979**, *A35*, 63.
(11) *International Tables for X-ray Crystallography*; Kynoch: Birmingham, England, 1974; Vol. IV.

Table VII. Bond Distances (Å) and Angles (deg) of $(n\text{-}Bu_4N)_2[(Mo_6X_7Y)Cl_6]$ (X, Y = Cl, S; Cl, Se; Br, S; Mo_6,13+)[a]

	X, Y				X, Y		
	Cl, S	Cl, Se	Br, S		Cl, S	Cl, Se	Br, S
			Distances				
Mo(1)–Mo(2)	2.623 (1)	2.629 (1)	2.645 (2)	Mo(2)–X(2)	2.466 (2)	2.493 (2)	2.589 (3)
Mo(1)–Mo(3)	2.632 (1)	2.634 (1)	2.659 (2)	Mo(2)–X(3)	2.474 (2)	2.489 (2)	2.603 (3)
Mo(1)–Mo(2′)	2.626 (1)	2.626 (1)	2.653 (2)	Mo(2)–X(4)	2.471 (2)	2.486 (2)	2.586 (3)
Mo(1)–Mo(3′)	2.614 (1)	2.616 (1)	2.648 (2)	Mo(3)–X(1)	2.468 (2)	2.492 (2)	2.601 (3)
Mo(2)–Mo(3)	2.623 (1)	2.627 (1)	2.643 (3)	Mo(3)–X(2′)	2.461 (2)	2.486 (2)	2.596 (3)
Mo(2)–Mo(3′)	2.636 (1)	2.638 (1)	2.663 (2)	Mo(3)–X(3)	2.476 (2)	2.493 (2)	2.603 (3)
av Mo–Mo	2.626 (3)	2.628 (3)	2.653 (3)	Mo(3)–X(4)	2.467 (2)	2.479 (2)	2.579 (3)
Mo(1)–X(1)	2.474 (2)	2.500 (2)	2.608 (3)	av Mo–X	2.470 (2)	2.490 (3)	2.596 (4)
Mo(1)–X(2)	2.476 (2)	2.517 (2)	2.610 (3)	Mo(1)–Cl(1)	2.423 (2)	2.423 (2)	2.426 (5)
Mo(1)–X(3′)	2.471 (2)	2.487 (2)	2.599 (3)	Mo(2)–Cl(2)	2.422 (2)	2.415 (3)	2.420 (6)
Mo(1)–X(4)	2.461 (2)	2.476 (2)	2.570 (3)	Mo(3)–Cl(3)	2.425 (2)	2.421 (2)	2.427 (6)
Mo(2)–X(1′)	2.469 (2)	2.486 (2)	2.605 (3)	av Mo–Cl	2.423 (1)	2.421 (2)	2.425 (2)
			Angles				
Mo(2)–Mo(1)–Mo(3)	59.87 (2)	59.88 (2)	59.76 (6)	X(1)–Mo(1)–X(3′)	89.80 (6)	89.76 (6)	89.91 (9)
Mo(1)–Mo(2)–Mo(3)	60.22 (2)	60.17 (3)	60.39 (7)	X(1)–Mo(1)–X(4)	89.40 (6)	89.50 (6)	89.51 (9)
Mo(1)–Mo(3)–Mo(2)	59.90 (2)	59.95 (2)	59.85 (6)	X(2)–Mo(1)–X(3)	90.22 (6)	90.23 (6)	90.40 (9)
Mo(2)–Mo(1)–Mo(3′)	60.43 (2)	60.39 (2)	60.41 (6)	X(2)–Mo(1)–X(4)	90.14 (6)	90.15 (6)	90.13 (9)
Mo(1)–Mo(2)–Mo(3′)	59.62 (2)	59.57 (2)	59.85 (6)	X(1′)–Mo(2)–X(2)	89.13 (6)	88.81 (6)	89.12 (9)
Mo(1)–Mo(3′)–Mo(2)	59.95 (2)	60.04 (2)	59.74 (6)	X(1′)–Mo(2)–X(3)	89.84 (6)	90.04 (6)	89.91 (9)
Mo(2′)–Mo(1)–Mo(3)	60.17 (2)	60.20 (2)	60.16 (6)	X(2)–Mo(2)–X(4)	90.13 (5)	90.46 (6)	90.23 (9)
Mo(1)–Mo(2′)–Mo(3)	60.03 (2)	60.06 (2)	60.04 (6)	X(3)–Mo(2)–X(4)	90.39 (6)	90.31 (6)	90.70 (9)
Mo(1)–Mo(3)–Mo(2′)	59.80 (2)	59.74 (2)	59.80 (6)	X(1)–Mo(3)–X(2′)	89.25 (6)	88.84 (6)	89.06 (9)
Mo(2)–Mo(1′)–Mo(3)	60.06 (2)	60.14 (2)	59.81 (6)	X(1)–Mo(3)–X(4)	89.40 (6)	89.60 (6)	89.48 (9)
Mo(1′)–Mo(2)–Mo(3)	59.75 (2)	59.75 (2)	60.00 (6)	X(2′)–Mo(3)–X(3)	90.43 (6)	90.83 (6)	90.59 (9)
Mo(1′)–Mo(3)–Mo(2)	60.19 (2)	60.11 (2)	60.19 (6)	X(3)–Mo(3)–X(4)	90.45 (6)	90.39 (6)	90.82 (9)
Mo(1)–X(1)–Mo(2′)	64.18 (5)	63.57 (5)	61.16 (7)	X(1)–Mo(1)–Cl(1)	93.54 (6)	93.30 (7)	92.32 (14)
Mo(1)–X(1)–Mo(3)	64.35 (5)	63.71 (5)	61.40 (7)	X(2)–Mo(1)–Cl(1)	92.02 (6)	91.77 (7)	89.92 (14)
Mo(2′)–X(1)–Mo(3)	64.53 (5)	64.01 (5)	61.53 (7)	X(3′)–Mo(1)–Cl(1)	91.97 (6)	91.77 (7)	90.64 (14)
Mo(1)–X(2)–Mo(2)	64.12 (4)	63.29 (4)	61.16 (8)	X(4)–Mo(1)–Cl(1)	92.55 (6)	92.35 (7)	90.62 (14)
Mo(1)–X(2)–Mo(3′)	63.95 (4)	63.06 (4)	61.14 (7)	X(1′)–Mo(2)–Cl(2)	93.87 (6)	93.33 (7)	91.80 (15)
Mo(2)–X(2)–Mo(3′)	64.67 (4)	63.98 (4)	61.77 (7)	X(2)–Mo(2)–Cl(2)	93.94 (6)	93.31 (7)	91.74 (15)
Mo(1′)–X(3)–Mo(2)	64.14 (4)	63.69 (5)	61.31 (7)	X(3)–Mo(2)–Cl(2)	91.08 (6)	90.84 (7)	89.34 (15)
Mo(1′)–X(3)–Mo(3)	63.80 (5)	63.38 (5)	61.20 (7)	X(4)–Mo(2)–Cl(2)	91.91 (6)	91.82 (7)	90.39 (15)
Mo(2)–X(3)–Mo(3)	63.98 (4)	63.64 (5)	61.02 (7)	X(1)–Mo(3)–Cl(3)	94.73 (6)	94.49 (7)	93.00 (15)
Mo(1)–X(4)–Mo(2)	64.26 (4)	63.99 (5)	61.72 (8)	X(2′)–Mo(3)–Cl(3)	92.35 (6)	91.88 (7)	90.82 (15)
Mo(1)–X(4)–Mo(3)	64.55 (4)	64.24 (5)	62.17 (7)	X(3)–Mo(3)–Cl(3)	90.50 (6)	90.14 (7)	88.76 (15)
Mo(2)–X(4)–Mo(3)	64.15 (4)	63.89 (5)	61.55 (7)	X(4)–Mo(3)–Cl(3)	92.83 (6)	92.45 (7)	91.27 (15)

[a] Key: (′) $-x, -y, -z$.

Figure 2 shows the crystal structure of $(n\text{-}Bu_4N)_2[(Mo_6Cl_7S)Cl_6]$ (Mo_6,13+), which is isomorphous with $(n\text{-}Bu_4N)_2[(Mo_6Cl_7Se)Cl_6]$ (Mo_6,13+) and $(n\text{-}Bu_4N)_2[(Mo_6Br_7S)Cl_6]$ (Mo_6,13+). Bond distances and angles of each compound are listed in Table VII. Sulfur and selenium atoms are statistically disordered over the eight capping sites in each compound.

Tetra-*n*-butylammonium salts of the three Mo_6(13+) clusters have isomorphous monoclinic unit cells with $(n\text{-}Bu_4N)_2[(W_6Cl_8)Cl_6]$ (W_6,12+) and $(n\text{-}Bu_4N)_2[(W_6Br_8)Br_6]$ (W_6,12+), and the cesium salts of $[(Mo_6Cl_7S)Cl_6]^{3-}$ (Mo_6,12+),[9] $[(Mo_6Cl_7Se)Cl_6]^{3-}$ (Mo_6,12+),[9] and $[(Mo_6Cl_6Se_2)Cl_6]^{3-}$ (Mo_6,13+)[12] have isomorphous triclinic unit cells. The crystal structures of these hexametal clusters must be controlled by the overall charge and the kind of counterion of the cluster complexes rather than by the formal oxidation number of the hexametal core.

The average bond distances in several Mo_6 clusters are listed in Table VIII. The average Mo–Mo distance in $[(Mo_6Cl_7S)Cl_6]^{2-}$ (Mo_6,13+) is very similar to that in $[(Mo_6Cl_7Se)Cl_6]^{2-}$ (Mo_6,13+). The Mo–Mo distances in these Mo_6(13+) clusters are slightly longer (0.016–0.017 Å) than those in the Mo_6(12+) clusters of corresponding ligand set. The average Mo–Mo distance in the bromide–sulfide capped cluster with the Mo_6(13+) state is 0.015 Å longer than those in the Mo_6(12+) species with the same ligands. It is 0.027 Å longer than those in Mo_6(13+) species with chloride–sulfide capping ligands.

The longer Mo–Mo distances in the Mo_6(13+) species compared to those in Mo_6(12+) are explained by the loss of one electron from the bonding orbitals.[14] A similar trend is observed between $[(W_6Br_8)Br_6]^{2-}$ (W_6,12+; 2.635 Å)[15] and $[(W_6Br_8)Br_6]^{-}$ (W_6,13+; 2.649 Å).[16] The longer Mo–Mo distance in $[(Mo_6Br_7S)Cl_6]^{2-}$ (Mo_6,13+) than those in $[(Mo_6Cl_7S)Cl_6]^{2-}$

Table VIII. Average Bond Distances (Å) in Selected Mo_6 Clusters

complexes[a]	Mo–Mo	Mo–X_c[b]	Mo–Cl_t[c]
	Mo_6(12+)		
$(H_3O)_2[(Mo_6Cl_8)Cl_6]\cdot 6H_2O$[d]	2.595 (4)	2.46 (1)	2.406 (7)
$(TMTTF)_2[(Mo_6Cl_8)Cl_6]$[e]	2.607 (2)	2.472 (2)	2.424 (3)
$(pyH)_3[(Mo_6Cl_7S)Cl_6]$[f]	2.604 (2)	2.473 (4)	2.454 (4)
$(pyH)_3[(Mo_6Cl_7S)Cl_6]\cdot 3pyHCl$[f]	2.610 (2)	2.475 (5)	2.456 (3)
$Cs_3[(Mo_6Cl_7S)Cl_6]\cdot H_2O$[g]	2.609 (2)	2.479 (2)	2.468 (5)
$Cs_3[(Mo_6Cl_7Se)Cl_6]\cdot H_2O$[g]	2.612 (3)	2.501 (3)	2.471 (6)
$(Et_4N)_3[(Mo_6Br_7S)Cl_6]$[h]	2.638 (6)	2.606 (6)	2.464 (14)
	Mo_6(13+)		
$(n\text{-}Bu_4N)_2[(Mo_6Cl_7S)Cl_6]$[h]	2.626 (3)	2.470 (2)	2.423 (1)
$(n\text{-}Bu_4N)_2[(Mo_6Cl_7Se)Cl_6]$[h]	2.628 (3)	2.490 (3)	2.421 (2)
$(n\text{-}Bu_4N)_2[(Mo_6Br_7S)Cl_6]$[h]	2.653 (3)	2.596 (4)	2.425 (2)

[a] $TMTTF^+$ = tetramethyltetrathiafulvalenium ion, py = C_6H_5N, Et = C_2H_5, Bu = C_4H_9. [b] X_c is the capping ligand. [c] Cl_t is the terminal chloride ion. [d] Reference 6. [e] Reference 7. [f] Reference 13. [g] Reference 9. [h] This work.

(12) Ebihara, M.; Kawamura, T.; Sasaki, Y.; Toriumi, K.; Saito, K. Unpublished result.
(13) Michel, J. B.; McCarley, R. E. *Inorg. Chem.* **1982**, *21*, 1864.
(14) (a) Azumi, T.; Saito, Y. *J. Phys. Chem.* **1988**, *92*, 1715. (b) Bursten, B. E.; Cotton, F. A.; Stanley, G. G. *Isr. J. Chem.* **1980**, *19*, 132. (c) Guggenberger, L. J.; Sleight, A. W. *Inorg. Chem.* **1969**, *8*, 2041.
(15) Zietlow, T. C.; Schaefer, W. P.; Sadeghi, B.; Hua, N.; Gray, H. B. *Inorg. Chem.* **1986**, *25*, 2195.
(16) Zietlow, T. C.; Schaefer, W. P.; Sadeghi, B.; Nocera, D. G.; Gray, H. B. *Inorg. Chem.* **1986**, *25*, 2198.

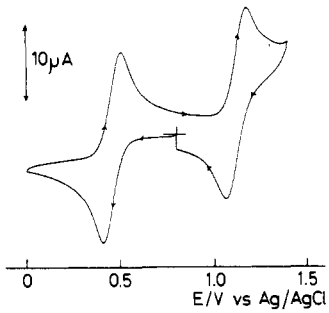

Figure 3. Cyclic voltammogram of $(n\text{-}Bu_4N)_2[(Mo_6Br_7S)Cl_6]$ (Mo_6,13+) in dichloromethane: scan rate, 100 mV/s; working electrode, glassy carbon; counter electrode, platinum; reference electrode, Ag/AgCl; 1×10^{-3} M salt in 0.1 M $n\text{-}Bu_4NClO_4$.

Table IX. Electrochemical Data for Mo_6(13+) Clusters

complexes	$E_{1/2}$, V vs Fc/Fc^{+} [a] (in CH_2Cl_2) 12+/13+	13+/14+	$E_{1/2}$, V vs Fc/Fc^{+} [b] (in CH_3CN) 12+/13+
$[(Mo_6Cl_7S)Cl_6]^{2-}$	+0.14	+0.9[c]	+0.28
$[(Mo_6Cl_7S)Br_6]^{2-}$	+0.18	+0.9[c]	+0.33
$[(Mo_6Cl_7Se)Cl_6]^{2-}$	+0.11	+0.8[c]	+0.23
$[(Mo_6Cl_7Se)Br_6]^{2-}$	+0.17	+0.8[c]	+0.28
$[(Mo_6Br_7S)Cl_6]^{2-}$	−0.11	+0.56	+0.14

[a] $E_{1/2}$ values measured by use of an Ag/AgCl reference electrode are related to the Fc/Fc^{+} potential measured in the same media. [b] $E_{1/2}$ values measured for Mo_6 (12+) species by use of an Ag/0.1 M $AgNO_3$ reference electrode are related to Fc/Fc^{+}. [c] The potential was not determined accurately because of a decomposition reaction.

(Mo_6,13+) and $[(Mo_6Cl_7Se)Cl_6]^{2-}$ (Mo_6,13+) must result from the "matrix effect"[17] due to the larger bromide ion since the Mo–Mo distance in $[(Mo_6Br_7S)Cl_6]^{3-}$ (Mo_6,12+) is longer than that in $[(Mo_6Cl_7S)Cl_6]^{3-}$ (Mo_6,12+).

The average Mo–Cl_t (Cl_t = terminal chloride) distances in Mo_6(13+) (2.421 (2)–2.425 (2) Å) are shorter than those in the Mo_6(12+) clusters with the mixed capping ligands (2.454 (4)–2.471 (6) Å) and are similar to those in $[(Mo_6Cl_8)Cl_6]^{2-}$ (Mo_6,12+). Such a difference is explained by the electrostatic attraction between $Mo_6X_7Y^{n+}$ and Cl^{-}.

The average Mo–X_c (X_c = capping ligand) distance of each Mo_6(13+) cluster complex is slightly shorter than that in the Mo_6(12+) with the same ligands, but the difference is not so large as that in Mo–Cl_t. The contraction may result not only from electrostatic attraction but also from electronic structural change.

Cyclic Voltammetry. Figure 3 shows the cyclic voltammogram (CV) of $[(Mo_6Br_7S)Cl_6]^{2-}$ (Mo_6,13+) in CH_2Cl_2 solution. Two quasi-reversible wave corresponding to an oxidation and a reduction process are observed. The reduction process must correspond to the change from Mo_6(13+) to Mo_6(12+). The oxidation process is regarded as a one-electron step, Mo_6(13+) to Mo_6(14+), on the basis of the comparison of peak current with that at the reduction process. Similar oxidation processes are observed for all other cluster complexes, but the potentials are not determined accurately since these processes are close to the following decomposition step. Electrochemical data are summarized in Table IX.

The $E_{1/2}$ values of $(n\text{-}Bu_4N)_3[(Mo_6X_7Y)X'_6]$ (Mo_6,12+) in CH_3CN[9] are also included in Table IX for comparison. The redox potential of Mo_6(13+) to Mo_6(12+) depends on the solvent. The redox potentials of the 12+/13+ stage in CH_2Cl_2 are slightly negative compared to those in CH_3CN. The oxidation of Mo_6(13+) to Mo_6(14+) in CH_3CN causes decomposition of the Mo_6 unit in all the cluster complexes. On the other hand, the oxidation of Mo_6(13+) to Mo_6(14+) is observed as a chemically reversible wave in CH_2Cl_2. The reason for such a difference is not clear, but there is a possibility to obtain $[(Mo_6Br_7S)Cl_6]^{-}$ (Mo_6,14+) by an oxidation reaction in CH_2Cl_2.

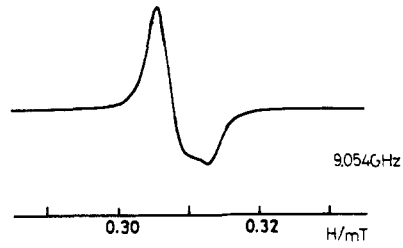

Figure 4. ESR spectrum of $(n\text{-}Bu_4N)_2[(Mo_6Cl_7S)Cl_6]$ (Mo_6,13+) in frozen (77 K) HCl/CH_3OH (1/10 v/v).

Table X. g Values of Mo_6(13+) Clusters at 77 K

complexes	$g_\perp$	$g_\parallel$
$[(Mo_6Cl_7S)Cl_6]^{2-}$ [a]	2.12	2.05
$[(Mo_6Cl_7S)Br_6]^{2-}$ [a]	2.12	2.05
$[(Mo_6Cl_7Se)Cl_6]^{2-}$ [b]	2.15	2.05
$[(Mo_6Cl_7Se)Br_6]^{2-}$ [b]	2.15	[c]
$[(Mo_6Br_7S)Cl_6]^{2-}$ [d]	2.13	2.07

[a] In frozen $CH_3CN/C_6H_5CH_3$ (1/1 v/v) solution. [b] In frozen CH_2Cl_2 solution. [c] Too broad to identify the parallel peak. [d] In frozen HCl/CH_3OH (1/10 v/v) solution.

The cyclic voltammogram of the Mo_6(13+) species is quasi-reversible in CH_3CN but changes with time. The anion $[(Mo_6Cl_7S)Cl_6]^{2-}$ (Mo_6,13+) gives only a one-electron reduction wave in CH_3CN immediately after dissolution. The wave has the same pattern as that of the oxidation wave of the Mo_6(12+) species, and the $E_{1/2}$ value is +0.14 V vs Fc/Fc^{+}. When the solution was aged in the absence of air and water, a new quasi-reversible peak appears at 0.35 V vs Fc/Fc^{+}, and the intensity of the old peak decreases. This change accompanies the change of electronic spectra. Other cluster complexes give similar changes of the CV in CH_3CN at a greater or smaller rate.

The time dependence of CV in CH_3CN solution may be ascribed to the formation of a solvolyzed cluster complex in the reduced form, $[(Mo_6Cl_7S)Cl_5(CH_3CN)]^{-}$ (Mo_6,12+). The reason is as follows. No time-dependent change of CV is observed in CH_2Cl_2 solution. The characteristic UV absorption peaks of $[(Mo_6Cl_7S)Cl_6]^{2-}$ (Mo_6,13+) decrease in CH_3CN. The difference of $E_{1/2}$ values between the two waves observed for the aged CH_3CN solution is similar to that between $[(Mo_6Br_7S)Cl_6]^{3-}$ and $[(Mo_6Br_7S)Cl_5(CH_3CN)]^{2-}$ in CH_3CN, which was isolated as the tetra-*n*-butylammonium salt.[18] Although the mechanism of formation of solvolyzed cluster is unknown, these observations suggest a possibility of synthesis of cluster complexes which have one terminal acetonitrile ligand, $[(Mo_6X_7Y)X_5(CH_3CN)]^{2-}$, from Mo_6(13+) species.

ESR Spectra. The ESR spectra in frozen HCl/CH_3OH (1/10 v/v) and frozen $CH_3CN/C_6H_5CH_3$ (1/1 v/v) solution are measured soon after dissolution. Figure 4 shows the ESR spectrum of $[(Mo_6Cl_7S)Cl_6]^{2-}$ in frozen $CH_3CN/C_6H_5CH_3$ solution at 77 K. The spectrum pattern remains unchanged as temperature is lowered to 10 K. The signal is explained as an axially symmetric $S = {}^1/_2$ system with no hyperfine splitting. The **g**-tensor values of five clusters (Table X) are quite similar to each other and are slightly larger than those of electrochemically generated $[(Mo_6Cl_8)Cl_6]^{-}$ (Mo_6,13+) ($g_\perp = 2.10$, $g_\parallel = 2.0$).

The ESR data indicate that the HOMO of these Mo_6(13+) clusters is nondegenerated. Possible HOMO's of O_h symmetrical $Mo_6X_8^{4+}$ clusters are all degenerated (e.g. e_g, t_{2u}, t_{2g}).[14] Gray et al. pointed out, on the basis of its axially symmetric ESR data, that the depopulation of an e_g HOMO caused a tetragonal distortion on the electrochemical oxidation of the hexamolybdenum cluster complex capped by chlorides.[2a] Introduction of one capping chalcogenide ligand can bring about a distortion of the Mo_6 skeleton from O_h symmetry even in the Mo_6(12+) state. The open-shell electronic state of a Mo_6(13+) cluster can also be an

(17) Corbett, J. D. *J. Solid State Chem.* **1981**, *37*, 335.

(18) Ebihara, M.; Kawamura, T.; Isobe, K.; Saito, K. Unpublished result.

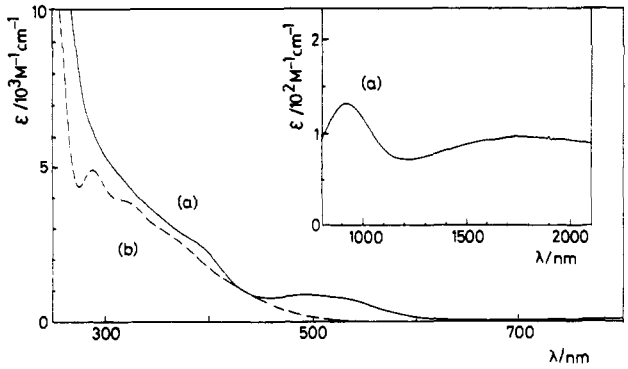

Figure 5. Electronic absorption spectra of $(n\text{-}Bu_4N)_2[(Mo_6Cl_7S)Cl_6]$ (Mo_6,13+; a) and $(n\text{-}Bu_4N)_3[(Mo_6Cl_7S)Cl_6]$ (Mo_6,12+; b) in dichloromethane.

Table XI. Electronic Absorption Peaks of Tetra-*n*-butylammonium Salts (Mo_6,13+) in Dichloromethane

complexes	λ, nm	ν, cm^{-1}	ε, M^{-1} cm^{-1}
$[(Mo_6Cl_7S)Cl_6]^{2-}$	1750	5710	95
	919	10900	129
	489	20400	959
$[(Mo_6Cl_7S)Br_6]^{2-}$	1750	5710	117
	949	10500	207
	562	17800	1410
$[(Mo_6Cl_7Se)Cl_6]^{2-}$	1700	5880	101
	889	11200	129
	609	16400	915
$[(Mo_6Cl_7Se)Br_6]^{2-}$	1650	6060	142
	923	10800	204
	648	15400	1310
$[(Mo_6Br_7S)Cl_6]^{2-}$	1900	5260	94
	929	10800	108
	515	19400	868

origin of distortion. We were unable to detect the molecular distortion from the X-ray structure determination because of the disorder of our complexes in the crystal. The similarity of the present ESR spectral pattern to those observed by Gray et al., however, indicates a possibility of a similar distortion of the hexametal core with the mixed capping ligands.

Electronic Absorption Spectra. Figure 5 compares the electronic absorption spectrum of $(n\text{-}Bu_4N)_2[(Mo_6Cl_7S)Cl_6]$ (Mo_6,13+) with that of $(n\text{-}Bu_4N)_3[(Mo_6Cl_7S)Cl_6]$ (Mo_6,12+) in CH_2Cl_2. The former gives three absorption peaks in the range 400–2200 nm, which are not observed in the latter. Other cluster complexes with the Mo_6(13+) core also have three absorption peaks in this region (480–650, ~900, and ~1800 nm). Absorption spectra of the five Mo_6(13+) complexes in the visible region are exemplified in Figure 6. Absorption peaks and their absorption coefficients are summarized in Table XI.

The peaks of Mo_6(13+) species in the 900- and 1800-nm regions are little affected by the change of capping and terminal ligands and have small ε values (ca. 100 M^{-1} cm^{-1}). These facts imply that the bands are due to the transition from a doubly-occupied Mo–Mo bonding orbital to the half-occupied Mo–Mo bonding orbital.

The position of the peaks of Mo_6(13+) species in the range of 480–650 nm depends on both the capping and the terminal ligands. When the capping chlorides are replaced by bromide in $[(Mo_6Cl_7S)Cl_6]^{2-}$, the peak gives a red shift by 1000 cm^{-1}. Substitution of bromide for the terminal chlorides in $[(Mo_6Cl_7S)Cl_6]^{2-}$ causes a larger red shift (2600 cm^{-1}) of the band. The replacement of the capping sulfide by a selenide gives a much

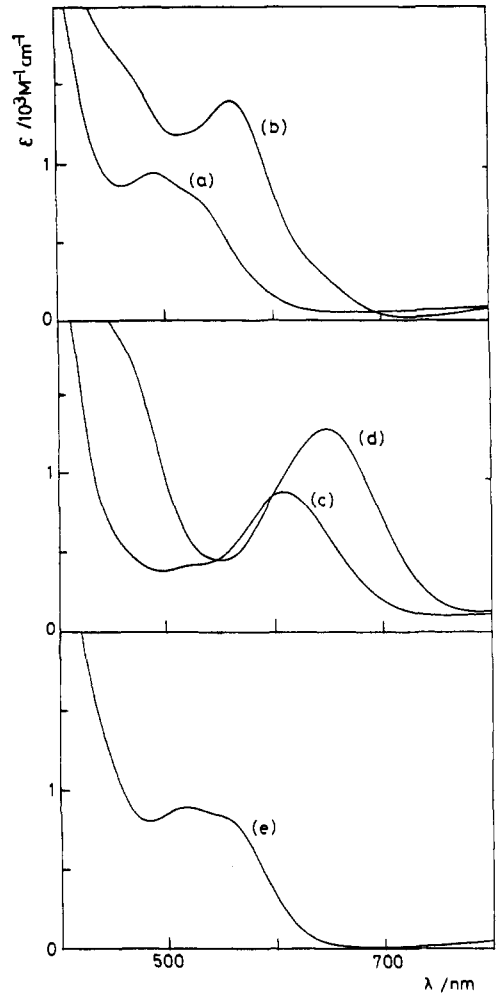

Figure 6. Electronic absorption spectra of $(n\text{-}Bu_4N)_2[(Mo_6X_7Y)X'_6]$ (Mo_6,13+) in dichloromethane: (a) $[(Mo_6Cl_7S)Cl_6]^{2-}$; (b) $[(Mo_6Cl_7S)Br_6]^{2-}$; (c) $[(Mo_6Cl_7Se)Cl_6]^{2-}$; (d) $[(Mo_6Cl_7Se)Br_6]^{2-}$; (e) $[(Mo_6Br_7S)Cl_6]^{2-}$.

larger red shift (4000 cm^{-1}). These band must be due to the ligand to metal charge transfer because they have large ε value and depend on the capping and terminal ligands.

In Mo_6(13+) and W_6(13+) cluster complexes with eight capping ligands no absorption band was reported in the range 800–2200 nm. This work provides first observation of the absorption band in this region for the Mo_6(13+) complexes.

Acknowledgment. We wish to thank Professor T. Kawamura (Gifu University) and Professor T. Ito (Tohoku University) for useful discussion and Dr. S. Kawata (Tohoku University) and Dr. H. Ohshio (IMS) for ESR measurements.

Registry No. $(n\text{-}Bu_4N)_2[(Mo_6Cl_7S)Cl_6]$, 139942-91-9; $(n\text{-}Bu_4N)_2[(Mo_6Cl_7Se)Cl_6]$, 139942-89-5; $(n\text{-}Bu_4N)_2[(Mo_6Br_7S)Cl_6]$, 139942-97-5; $(Et_4N)_3[(Mo_6Br_7S)Cl_6]$, 139914-15-1; $(n\text{-}Bu_4N)_3[(Mo_6Cl_7S)Cl_6]$, 111025-64-0; $(n\text{-}Bu_4N)_3[(Mo_6Cl_7Se)Cl_6]$, 111025-68-4; $(n\text{-}Bu_4N)_2[(Mo_6Cl_7Se)Br_6]$, 139942-93-1; $(n\text{-}Bu_4N)_3[(Mo_6Br_7S)Cl_6]$, 111025-67-3; $(n\text{-}Bu_4N)_2[(Mo_6Cl_7S)Br_6]$, 139942-95-3.

Supplementary Material Available: Tables of all crystal data, final positional parameters and equivalent thermal parameters of countercations, and anisotropic thermal parameters and a figure showing absorption spectra of the UV and near-IR regions of all the complexes (10 pages); tables of calculated and observed structure factors (75 pages). Ordering information is given on any current masthead page.